Title

Crystal Structure Evolution and Notable Thermal Expansion in Hybrid Perovskites
Formamidinium Tin Iodide and Formamidinium Lead Bromide

Authors

Schueller, Emily C
Laurita, Geneva
Fabini, Douglas H
et al.

Peer reviewed

Crystal Structure Evolution and Notable Thermal Expansion in Hybrid Perovskites Formamidinium Tin Iodide and Formamidinium Lead Bromide

Emily C. Schueller,[†] Geneva Laurita,[‡] Douglas H. Fabini,[†]
Constantinos C. Stoumpos,[¶] Mercouri G. Kanatzidis,[¶] and Ram Seshadri[*,†,§]

[†]Materials Department and Materials Research Laboratory
University of California, Santa Barbara, California 93106, USA
[‡]Department of Chemistry and Biochemistry, Bates College, Lewiston, Maine 04240, United States
[¶]Department of Chemistry, and Argonne-Northwestern Solar Energy Research Center
Northwestern University, Evanston, Illinois 60208, USA
[§]Department of Chemistry and Biochemistry
University of California, Santa Barbara, California 93106, USA

E-mail: seshadri@mrl.ucsb.edu

Abstract

The temperature-dependent structure evolution of the hybrid halide perovskite compounds, formamidinium tin iodide (FASnI$_3$, FA$^+$ = CH[NH$_2$]$_2^+$) and formamidinium lead bromide (FAPbBr$_3$) has been monitored using high-resolution synchrotron X-ray powder diffraction between 300 K and 100 K. The data are consistent with a transition from cubic $Pm\bar{3}m$ (#221) to tetragonal $P4/mbm$ (#127) for both materials upon cooling; this occurs for FAPbBr$_3$ between 275 K and 250 K, and for FASnI$_3$ between 250 K and 225 K. Upon further cooling, between 150 K and 125 K, both materials undergo a transition to an orthorhombic $Pnma$ (#62) structure. The transitions are confirmed by calorimetry and dielectric measurements. In the tetragonal regime, the coefficients of volumetric thermal expansion of FASnI$_3$ and FAPbBr$_3$ are among the highest recorded for any extended inorganic crystalline solid, reaching 219 ppm K^{-1} for FASnI$_3$ at 225 K. Atomic displacement parameters of all atoms for both materials suggest dynamic motion is occurring in the inorganic sublattice due to the flexibility of the inorganic network and dynamic lone pair stereochemical activity on the B-site. Unusual pseudo-cubic behavior is displayed in the tetragonal phase of the FAPbBr$_3$, similar to that previously observed in FAPbI$_3$.

Introduction

Hybrid halide perovskites (formula ABX_3, where A is an organic cation, B is a divalent metal such as Sn or Pb, and X is a halide anion) have been the subject of renewed scientific interest since the first hybrid perovskite-based photovoltaic (PV) device in 2009.[1] This interest is due to their useful optoelectronic properties such as strong photoluminescence and long carrier lifetimes[2,3] and potential as high performance, low cost PV absorbers. Formamidinium lead iodide (FAPbI$_3$) is a component of the highest performing perovskite solar cells with power conversion efficiencies above 20%.[4,5] While there has been much research focused on improving device performance, less is known about the structure evo-

lution of these materials. Detailed understanding of the crystal structure could provide strong insight into the observed properties such as low recombination rates[6,7] and high defect tolerance[8,9] that lead to high photovoltaic performance in the hybrid halide perovskites.

Diffraction studies on the halide perovskites indicate that the materials usually distort from cubic to tetragonal to orthorhombic (and occasionally further to rhombohedral or monoclinic) upon cooling, following simple perovskite tilt systems.[10] $CsSnI_3$ transitions from $Pm\bar{3}m$ to $P4/mbm$ to $Pnma$ upon cooling from $500\,K$ to $300\,K$,[11] while $MAPbI_3$ (MA = CH_3NH_3) transitions from $Pm\bar{3}m$ to $I4/mcm$ to $Pnma$ upon cooling from $350\,K$ to $100\,K$.[12] Materials with more flexibility in the inorganic lattice and enhanced lone pair activity such as $MAPbCl_3$ can undergo more complex phase transitions; for example, the low temperature ordered phase of $MAPbCl_3$ is $Pnma$ but with highly distorted octahedra, not the simple tilt phase that would be expected for a more traditional perovskite.[13] A recent structural study on $FAPbI_3$ discovered that the material has one of the largest coefficients of volumetric thermal expansion (α_v) of any extended crystalline solid, $203\,ppm\,K^{-1}$ at $274\,K$.[14] $FAPbI_3$ also displays unusual reentrant behavior of a pseudo-cubic phase at low temperature; the phase transitions upon cooling go from $Pm\bar{3}m$ to $P4/mbm$ to pseudo-cubic $P4/mbm$, indicating complex interactions in this regime.[14] Locally, total scattering analysis using the pair distribution function technique on hybrid perovskites has revealed a highly flexible inorganic network with large local distortions among the $B-X$ octahedra in addition to dynamic lone pair stereochemical activity at high temperatures.[15–19]

We study herein the related compounds formamidinium tin iodide ($FASnI_3$) and formamidinium lead bromide ($FAPbBr_3$) in order to provide a more complete picture of the hybrid halide perovskite family and uncover trends that could lead to a deeper understanding of the class as a whole and possibly to a more rational design of high performance photovoltaic and optoelectronic materials. We build on what has already been reported in the literature[20] with the use of high resolution synchrotron data to elucidate subtle structural

3

changes that may have a large impact on the observed properties. We have determined the first phase transition upon cooling from room temperature to be cubic $Pm\bar{3}m$ to tetragonal $P4/mbm$ between 225 K and 250 K for FASnI$_3$ and between 250 K and 275 K for FAPbBr$_3$. A further phase transformation to orthorhombic $Pnma$ occurs between 125 K and 150 K for both materials. We have corroborated these phase transitions with calorimetry and dielectric measurements. FASnI$_3$ has an even higher value of α_v in the tetragonal phase than FAPbI$_3$ of 219 ppm K^{-1} at 225 K compared to 203 ppm K^{-1} at 274 K for FAPbI$_3$.[14] This presents an important engineering consideration for the incorporation of these materials in photovoltaic devices operating at various temperatures as relatively large volume changes are likely to occur over the operating temperature range of the device (at 300 K, α_v for FASnI$_3$ is still high at 174 ppm K^{-1}).

Experimental Methods

Formamidinium tin iodide (FASnI$_3$) and formamidinium lead bromide (FAPbBr$_3$) were prepared by a modification of previously reported procedures[20] which has been described in detail in Laurita *et al.*[16] High resolution synchrotron powder X-ray diffraction (XRD) data were collected at 25 K intervals from 90 K to 300 K using beamline 11-BM at the Advanced Photon Source (APS), Argonne National Laboratory with a wavelength of 0.4592 Å. 20 mg of ground sample was packed and sealed into a 0.5 mm OD Kapton capillary. Le Bail and Rietveld analyses were performed using the GSAS software suite[21] with the EXPGUI interface.[22] Crystal structures were visualized using the VESTA software suite.[23] Differential scanning calorimetry (DSC) was performed on approximately 5 mg samples under a nitrogen atmosphere from 100 K to 300 K on a TA Instruments DSC Q2000 at rates of 5 and 10 degrees per minute. Dielectric measurements were performed in a Quantum Design PPMS DynaCool from 300 K to 1.8 K with an Andeen-Hagerling AH 2700A capacitance bridge for capacitance and loss measurements. Dielectric permittivity values were

calculated from a flat plate capacitor model. Pellets for dielectric measurements were prepared by grinding a sample of material and pressing to 4 tons in a 6 mm cylindrical die (around 0.3 GPa) to obtain around 1.5 mm thick pellets. Electrodes were applied via low temperature indium soldering.

Results and Discussion

The structural evolution of FASnI$_3$ and FAPbBr$_3$ with temperature was analyzed from approximately 300 K to 100 K using X-ray diffraction data, and relevant structural parameters are tabulated in Tables 1 and 2. Phase transitions were determined by analysis of Bragg peak splitting and emergence. This work focuses on the inorganic sublattice, as dynamic disorder on the A-site and the smaller electron count of the organic cation add uncertainty when trying to assign A-site orientations from X-ray diffraction. Space groups were assigned by examining the "simple" octahedral tilt systems from the $Pm\bar{3}m$ cubic perovskite as enumerated by Howard and Stokes,[10] and all patterns were indexed well by one of these space groups. For data near phase transitions where the space group was somewhat ambiguous, fits to both space groups were performed and the fit with the lowest R-value was chosen. In order to determine whether the structure was actually lower symmetry but with a pseudo-symmetric unit cell, as has been suggested for these types of materials,[20] Bragg peak width analysis was performed on low-angle peaks and compared to peak widths of a known high symmetry structure, cubic FAPbI$_3$ with the space group $Pm\bar{3}m$, in which the only sources of broadening are instrumental resolution and sample size/strain, not overlapping peaks. In all cases, the peak widths were equal on the order of the resolution of the instrument. Because there was no detectable peak broadening or splitting, the higher symmetry space groups were retained.

The room temperature crystal structure of both materials is best fit by the cubic $Pm\bar{3}m$ perovskite structure, in agreement with findings from the original work on FASnI$_3$[24] and

single crystal work from Dang *et al.* [25] for FASnI$_3$ and several reports [26,27] for FAPbBr$_3$. The FAPbBr$_3$ transitions between 275 K and 250 K to a phase described by tetragonal $P4/mbm$ with FASnI$_3$ following between 250 K and 225 K. Upon further cooling, both materials distort to an orthorhombic $Pnma$ phase between 150 K and 125 K. Some groups have reported a space group of pseudo-cubic $Amm2$ for FASnI$_3$ at 300 K, [20,28,29] which has the same Bragg peak positions as $Pm\bar{3}m$ but with the ability to orient the asymmetric FA cations. However, $Amm2$ would have multiple overlapping peaks at each Bragg position, which was not evident upon visual inspection. In order to quantitatively compare the two structure determinations, we performed a fit to this space group which resulted in an R$_{wp}$ of 14.59% at 300 K versus 10.27% for $Pm\bar{3}m$ from high resolution synchrotron powder diffraction. Because of the lower symmetry, the $Amm2$ phase has more refinable parameters than $Pm\bar{3}m$. Therefore, a significantly worse R$_{wp}$ value for $Amm2$ than the $Pm\bar{3}m$ phase is probably due to difficulty assigning electron density to overlapping peaks. This, in combination with previously described peak width analysis of the (100) peak, indicates that the best fit to our data at room temperature is a $Pm\bar{3}m$ phase, although it is possible that other techniques that are better suited to looking at the formamidinium orientations could improve on this assignment. Additionally, at low temperatures and applied electric fields DFT calculations suggest ordering of the A-site cation could occur, [30] but these conditions were not probed by our experiments. The locations of the phase transitions are examined by DSC, shown in Figure 1(a) and (b). The high temperature phase transitions in both materials appear to be second order, while the low temperature transitions are accompanied by multiple peaks in the DSC, suggesting a complex cascade of phase transitions. Interestingly, the transition from tetragonal to orthorhombic in FASnI$_3$ appears more pronounced upon heating than upon cooling, shown in Figure 1(a). This suggests that there may be multiple pathways for forming the low temperature orthorhombic state but there is a more deterministic transition back to the tetragonal phase. The phase transitions can be seen in the X-ray diffraction data as emergence of new peaks upon cooling as shown in Figure

1(c) and (d), reflecting a lowering of the symmetry, with peaks appearing in the same temperature ranges as the expected phase transitions. However, we were able to resolve and refine only one low temperature phase transition from the XRD data.
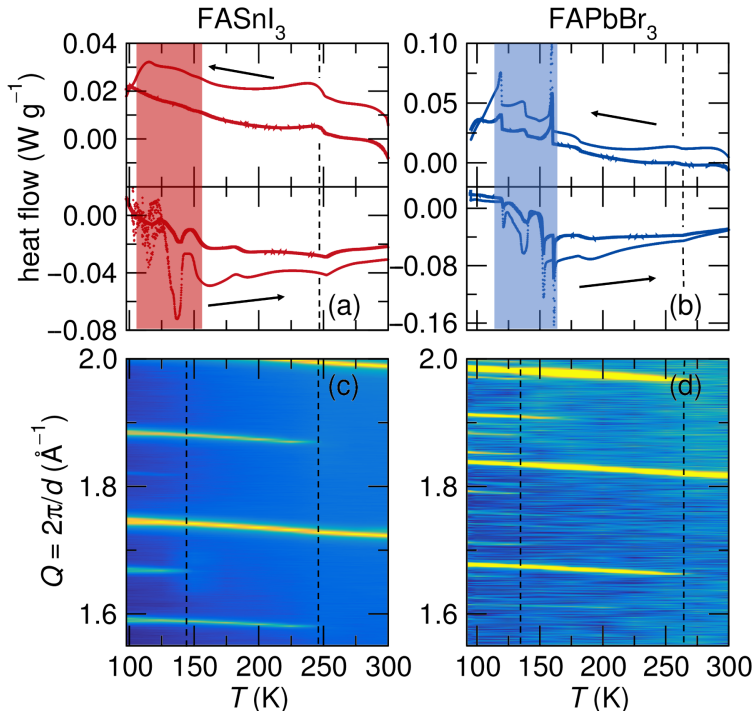

Figure 1: DSC from 100 K to 300 K confirms the presence of phase transitions for (a) FASnI$_3$ and (b) FAPbBr$_3$. The arrows indicate cooling and heating ramps. XRD data performed in the same temperature range for (c) FASnI$_3$ and (d) FAPbBr$_3$. Phase transitions upon cooling are signaled by the development of new peaks in the pattern, indicating a lowering of symmetry in the crystal structure. XRD patterns were taken at 25 K intervals and interpolated in between. A non-interpolated version is shown in the Supporting Information (Figure S1). Dashed lines are shown at the emergence of new XRD peaks to compare phase transition temperatures from DSC and XRD. Due to the complexity of the low temperature transition(s) in DSC, the regions of interest are shaded.

Rietveld refinement fits to the XRD data are shown in Figure 2. The fits were performed modeling the FA as a spherical atom with the same X-ray scattering power (Mn) for simplicity. This assumption is reasonable considering that in both compounds the FA has only around 10% of the total electrons, which means it has minimal scattering power, as the scattering power scales with the square of the electron density. However, because of this and dynamic disorder, the refined atomic displacement parameters (ADPs) on the cation
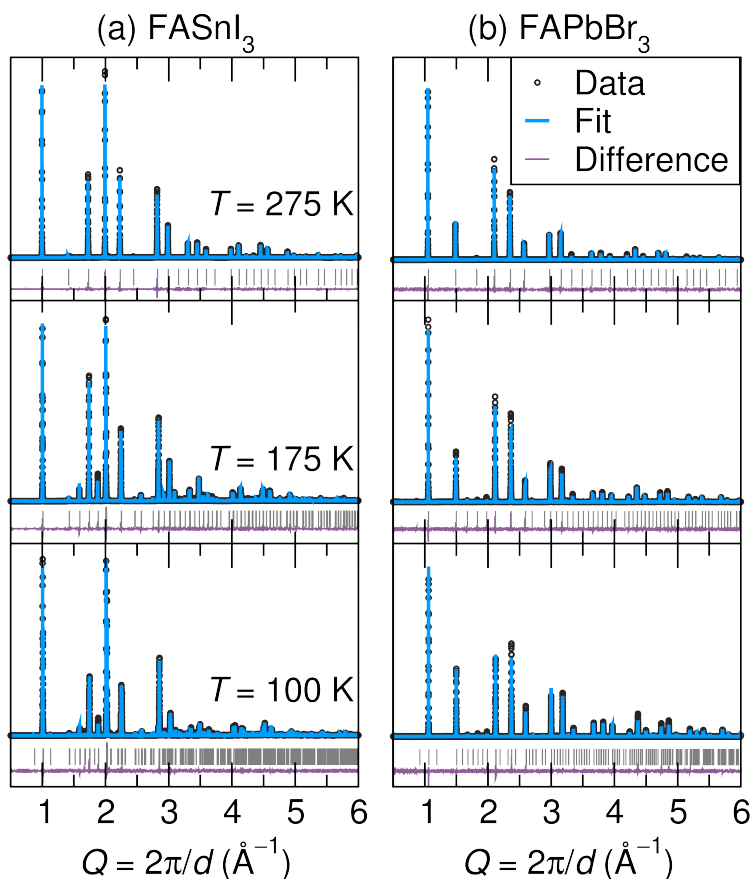
A-site are large.

Figure 2: Rietveld fits to synchrotron XRD data for (a) FASnI$_3$ and (b) FAPbBr$_3$. The data at 275 K is best fit to a cubic $Pm\overline{3}m$ phase, the 175 K data to a tetragonal $P4/mbm$ phase, and the 100 K data to an orthorhombic $Pnma$ phase for both samples.

Crystal structures throughout the phase evolution are shown in Figure 3 with ADPs shown at 50% probability ellipsoids. The halide ADPs are highly anisotropic, with motion occurring orthogonal to the $B - X$ bond, and decrease in size upon cooling. These remain anisotropic for both FASnI$_3$ and FAPbBr$_3$ at low temperatures, indicating dynamic local disorder and distortions of the octahedra, as seen in the literature.[15–19]

The ADPs on the B-site (Sn and Pb) are also large, further hinting at the presence of local disorder in the materials. The Sn ADP is consistently larger than that of the Pb, as seen in Figure 4(a). This trend aligns with the expected effects of lone pair stereochemical activity, which is predicted to be stronger for Sn^{2+} than Pb^{2+} due to deeper ns^2 levels in

8

Table 1: Crystallographic Data for FASnI$_3$

Empirical Formula	CH(NH$_2$)$_2$SnI$_3$		
Formula Weight (g mol^{-1})	544.49		
Source	11-BM Synchrotron		
Wavelength (Å)	0.4592		
Temperature (K)	100	175	275
Crystal System	Orthorhombic	Tetragonal	Cubic
Space Group (No.)	$Pnma$ (62)	$P4/mbm$ (127)	$Pm\bar{3}m$ (221)
a (Å)	8.81749(8)	8.86227(2)	6.30961(1)
b (Å)	12.41641(7)	/	/
c (Å)	8.8578(1)	6.24892(2)	/
V (Å^3)	969.773(9)	490.789(3)	251.1930(6)
Z	4	2	1
d-space range (Å^{-1})	0.888 – 7.211	0.891 – 6.267	0.892 – 6.310
χ^2	9.869	3.672	4.005
R_p (%)	11.85	7.69	7.83
R_{wp} (%)	17.73	10.67	11.03

Table 2: Crystallographic Data for FAPbBr$_3$

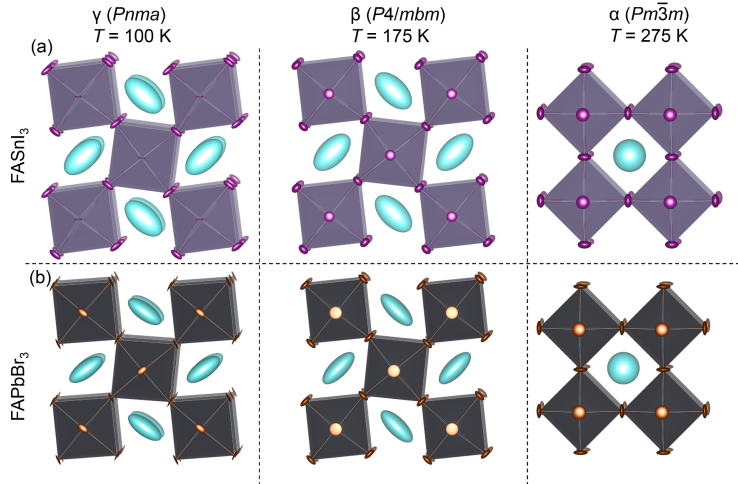| Empirical Formula	CH(NH$_2$)$_2$PbBr$_3$		
Formula Weight (g mol^{-1})	491.98		
Source	11-BM Synchrotron		
Wavelength (Å)	0.4592		
Temperature (K)	100	175	275
Crystal System	Orthorhombic	Tetragonal	Cubic
Space Group (No.)	$Pnma$ (62)	$P4/mbm$ (127)	$Pm\bar{3}m$ (221)
a (Å)	8.37433(9)	8.41525(5)	5.98618(2)
b (Å)	11.8609(1)	/	/
c (Å)	8.38073(9)	5.94735(8)	/
V (Å^3)	832.436(9)	421.170(3)	214.511(3)
Z	4	2	1
d-space range (Å^{-1})	0.888 – 6.844	0.892 – 5.950	0.892 – 5.986
χ^2	1.958	1.400	1.397
R_p (%)	13.27	11.42	11.37
R_{wp} (%)	17.40	14.13	14.09

Figure 3: Structural evolution of (a) FASnI$_3$ and (b) FAPbBr$_3$ with temperature. Atomic displacement parameters shown at 50% probability ellipsoids. The halides have highly anisotropic atomic displacement parameters, with motion orthogonal to the $B - X$ bond as observed in the literature[16,18] reflecting dynamic octahedral tilting as well as possible intra-octahedral distortions.

lead.[16,17,31] While the effects of lone pair stereochemical activity at elevated temperatures in these materials, labeled *emphanisis* in the chalcogenide literature,[32–34] are not correlated enough to induce an ordered distortion visible in the average structure diffraction pattern, the combination of anisotropic halide ADPs and elevated B-site ADPs in the high temperature phase hint at local dynamic distortions, which have been observed previously in tin and lead perovskites.[14,17,35,36] In addition to thermally activated lone pair activity, halide perovskites are known to have high flexibility within the inorganic octahedral network,[17,18,35] allowing for local octahedral tilting and contributing to the anisotropy in halide ADPs and elevated ADPs in all species. The monotonic decrease in size for all ADPs upon cooling suggests that the disorder is dynamic and thermally activated, rather than static.

FASnI$_3$ and FAPbBr$_3$ have remarkably high coefficients of volumetric thermal expansion for crystalline solids. It was recently found that FAPbI$_3$ has a high α_v of 203 ppm K^{-1} at 274 K,[14] but FASnI$_3$ has an even higher value of 219 ppm K^{-1} at 225 K as seen in Figure 5(a). While this must be taken into consideration for solar device performance, as this
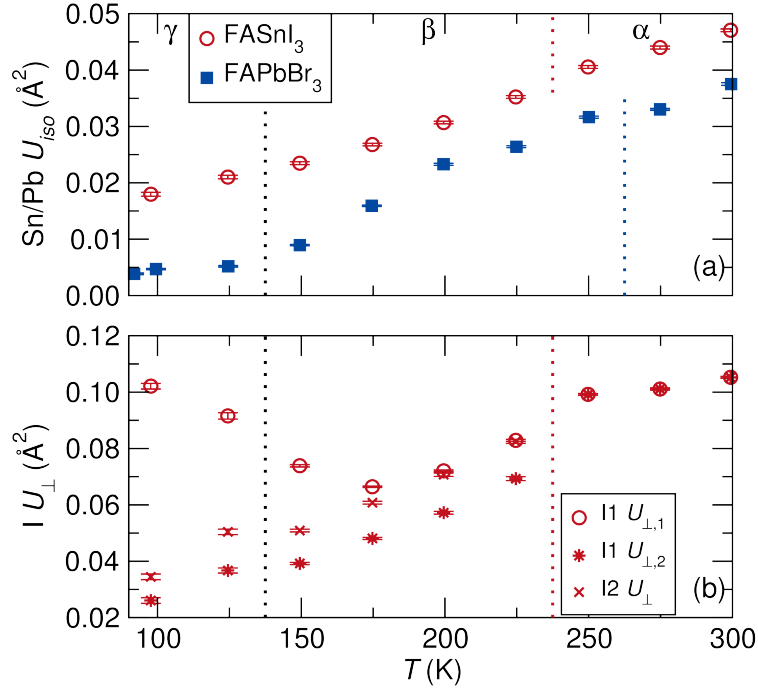
Figure 4: (a) Isotropic atomic displacement parameters (ADPs) for the B ion in the perovskites. The value for Sn is consistently larger than for Pb due to enhanced dynamic lone pair stereochemical activity. (b) Anisotropic halide ADP terms perpendicular to the $B - X$ bonds show expected behavior upon cooling for the iodide aside from one component which increases upon cooling in the orthorhombic phase, an indication of static disorder along that direction. However, no clear trend appears in the bromide (bromide ADPs not shown for clarity).

manifests in volume changes in the material over the normal operating temperature range, the novelty of one of the highest values of α_v yet seen in a crystalline solid is exciting.

Another odd feature in the structural evolution of these perovskites is seen in the particulars of the lattice parameters upon cooling. $FASnI_3$ exhibits expected trends in lattice parameters, but in $FAPbBr_3$ unusual behavior is displayed in the tetragonal phase, as seen in Figure 5(c). The ratio of $\tilde{a} = a/\sqrt{2}$ to $\tilde{c} = c$ is curiously close to 1 throughout the tetragonal phase, only increasing again at the orthorhombic phase transition. The normalized lattice parameters never deviate more than $0.005\,\text{Å}$ from each other in the tetragonal phase, indicating the crystal maintains a nearly cubic unit cell, while in $FASnI_3$ the deviations reach over $0.02\,\text{Å}$ in the tetragonal phase. Similar pseudo-cubic behavior was observed in $FAPbI_3$;[14] however, in $FAPbI_3$ it is reentrant in the tetragonal γ-phase, and no transition was fully completed to an orthorhombic structure by $100\,\text{K}$, whereas $FAPbBr_3$ does undergo a tetragonal to orthorhombic transition after further cooling. This unusual behavior happens in both formamidinium lead halide perovskites studied so far but not in the tin analogue, so it could be that the lead is somehow contributing to complex disorder in the tetragonal phase. At first glance, this would appear to be a size effect because Pb^{2+} is larger than Sn^{2+}, but $FASnI_3$ has larger lattice parameters than $FAPbBr_3$. This suggests the presence of a more subtle effect, such as ionicity of $B-X$ bonds impacting interactions with the formamidinium.

Figure 4(b) shows the anisotropic ADP components for the halides in the direction perpendicular to the bond. The size of most iodine ADP components consistently decrease with temperature as expected. The bromine ADPs, on the other hand, show no clear trends with temperature, another indicator of disorder in the material that is not fully captured by a crystallographic model.

Dielectric measurements were performed on $FAPbBr_3$ to obtain information about molecular cation motion in the material as shown in Figure 6. Due to the semiconducting nature of the sample, electronic conduction is too great above $200\,\text{K}$ to extract meaningful
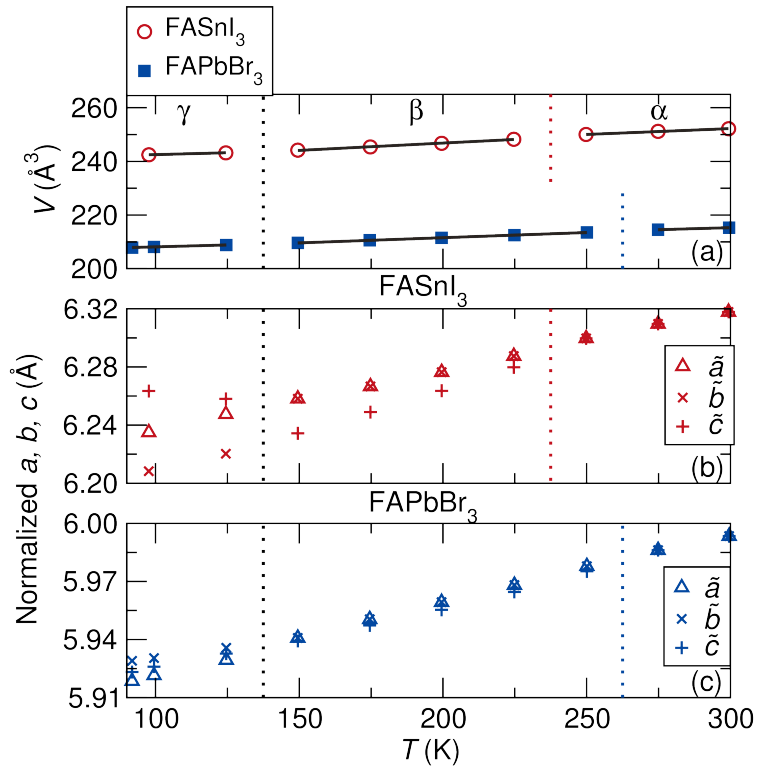
Figure 5: (a) Volumetric expansion in the materials shows that $FASnI_3$ has an extremely high α_v of $219\,\text{ppm}\,\text{K}^{-1}$ at $225\,\text{K}$. Normalized (pseudo-cubic) lattice parameters as a function of temperature in $FASnI_3$ (b) and $FAPbBr_3$ (c) show unusual behavior in the tetragonal phase of $FAPbBr_3$. Error bars are smaller than the markers and are omitted for clarity.

13

dielectric information about the cubic to tetragonal phase transition. The smaller band gap of FASnI$_3$ precluded the acquisition of dielectric properties using the capacitance method. Compared to similar materials such as MAPbI$_3$ and FAPbI$_3$,[37] FAPbBr$_3$ does not have an abrupt freezing of dipole rotation, indicated by a sudden drop in the real portion of the dielectric permittivity. While the magnitude of the real part of the permittivity is similar to that of MAPbBr$_3$ at low temperatures, the shape of the graph is far different, missing both the sudden drop as mentioned before and the upturn upon cooling at temperatures higher than the drop.[38] It appears as though FAPbBr$_3$ undergoes a more continuous slowing of molecular reorientation, possibly due to the smaller lattice parameters of FAPbBr$_3$, which could limit the motion of the formamidinium cation even at high temperatures, although it is possible that characteristic features could appear at temperatures above 200 K. The feature associated with the tetragonal to orthorhombic phase transition occurs in the same temperature region as phase transition signatures from DSC and XRD, further confirming the location of the phase transition.

We have utilized synchrotron XRD data to analyze the structure evolution of FASnI$_3$ and FAPbBr$_3$ with temperature from 300 K to 100 K. We observe that both materials undergo phase transformations from cubic $Pm\bar{3}m$ to $P4/mbm$ to $Pnma$ upon cooling and corroborate these transitions by calorimetry. A high value for α_v is observed in both materials, particularly in FASnI$_3$, giving it possibly the highest value of any extended crystalline solid near ambient temperatures. Large ADPs on the B-site cations along with highly anisotropic halide ADPs provide more evidence for local distortions and support observed *emphanisis* in tin and lead perovskites. Despite the impressive photovoltaic performance of hybrid halide perovksites, the large coefficient of volumetric thermal expansion presents a significant engineering challenge that must be taken into consideration when utilizing these materials in devices.
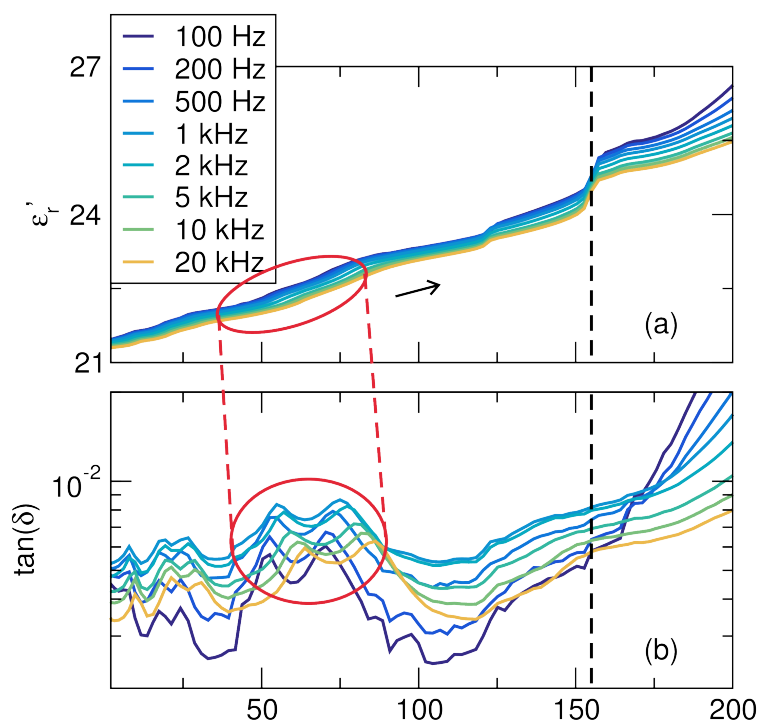
Figure 6: (a) The real part of the relative permittivity, ϵ_r', upon heating for FAPbBr$_3$ at various frequencies. (b) The loss tangent for FAPbBr$_3$ upon heating. The frequency disperse (spread over temperature) peaks in the loss tangent, indicated by a red ellipse, show the glassy freeze-out of the molecule, characterized by resonance between the dielectric relaxation process and the probe frequency. The absence of a sharp drop in the dielectric constant indicates dipole reorientation of the formamidinium is relatively hindered throughout the temperature range sampled. The dashed line shows the feature associated with the tetragonal to orthorhombic phase transitions and aligns with the temperature range from XRD and DSC.

15

Supporting Information Available: A non-interpolated version of Figure 1

Acknowledgement

References

(1) Kojima, A.; Teshima, K.; Shirai, Y.; Miyasaka, T. Organometal Halide Perovskites as Visible-Light Sensitizers for Photovoltaic Cells. *J. Am. Chem. Soc.* **2009**, *131*, 6050–6051.

(2) Deschler, F.; Price, M.; Pathak, S.; Klintberg, L. E.; Jarausch, D.-D.; Higler, R.; Hüttner, S.; Leijtens, T.; Stranks, S. D.; Snaith, H. J.; Atatre, M.; Phillips, R. T.; Friend, R. H. High Photoluminescence Efficiency and Optically Pumped Lasing in Solution-Processed Mixed Halide Perovskite Semiconductors. *J. Phys. Chem. Lett.* **2014**, *5*, 1421–1426.

(3) Tan, Z.-K.; Moghaddam, R. S.; Lai, M. L.; Docampo, P.; Higler, R.; Deschler, F.; Price, M.; Sadhanala, A.; Pazos, L. M.; Credgington, D.; Hanusch, F.; Bein, T.; Snaith, H. J.; Friend, R. H. Bright Light-Emitting Diodes Based on Organometal Halide Perovskite. *Nat. Nanotechnol.* **2014**, *9*, 687–692.

(4) Saliba, M.; Matsui, T.; Seo, J.-Y.; Domanski, K.; Correa-Baena, J.-P.; Nazeeruddin, M. K.; Zakeeruddin, S. M.; Tress, W.; Abate, A.; Hagfeldt, A.; Gratzel, M. Cesium-Containing Triple Cation Perovskite Solar Cells: Improved Stability, Reproducibility and High Efficiency. *Energy Environ. Sci.* **2016**, *9*, 1989–1997.

(5) Bi, D.; Tress, W.; Dar, M. I.; Gao, P.; Luo, J.; Renevier, C.; Schenk, K.; Abate, A.; Giordano, F.; Baena, J.-P. C.; Decoppet, J.-D.; Zakeeruddin, S. M.; Nazeeruddin, M. K.; Grätzel, M.; Hagfeldt, A. Efficient Luminescent Solar Cells Based on Tailored Mixed-Cation Perovskites. *Sci. Adv.* **2016**, *2*, e1501170.

(6) Wehrenfennig, C.; Eperon, G. E.; Johnston, M. B.; Snaith, H. J.; Herz, L. M. High Charge Carrier Mobilities and Lifetimes in Organolead Trihalide Perovskites. *Adv. Mater.* **2014**, *26*, 1584–1589.

(7) Oga, H.; Saeki, A.; Ogomi, Y.; Hayase, S.; Seki, S. Improved Understanding of the Electronic and Energetic Landscapes of Perovskite Solar Cells: High Local Charge Carrier Mobility, Reduced Recombination, and Extremely Shallow Traps. *J. Am. Chem. Soc.* **2014**, *136*, 13818–13825.

(8) Wu, X.; Trinh, M. T.; Niesner, D.; Zhu, H.; Norman, Z.; Owen, J. S.; Yaffe, O.; Kudisch, B. J.; Zhu, X.-Y. Trap States in Lead Iodide Perovskites. *J. Am. Chem. Soc.* **2015**, *137*, 2089–2096.

(9) Wetzelaer, G.-J. A. H.; Scheepers, M.; Sempere, A. M.; Momblona, C.; Ávila, J.; Bolink, H. J. Trap-Assisted Non-Radiative Recombination in Organic–Inorganic Perovskite Solar Cells. *Adv. Mater.* **2015**, *27*, 1837–1841.

(10) Howard, C. J.; Stokes, H. T. Group-Theoretical Analysis of Octahedral Tilting in Perovskites. *Acta Crystallogr. Sect. B* **1998**, *54*, 782–789.

(11) Chung, I.; Song, J.-H.; Im, J.; Androulakis, J.; Malliakas, C. D.; Li, H.; Freeman, A. J.; Kenney, J. T.; Kanatzidis, M. G. CsSnI$_3$: Semiconductor or Metal? High Electrical Conductivity and Strong Near-Infrared Photoluminescence from a Single Material. High Hole Mobility and Phase-Transitions. *J. Am. Chem. Soc.* **2012**, *134*, 8579–8587.

(12) Baikie, T.; Fang, Y.; Kadro, J. M.; Schreyer, M.; Wei, F.; Mhaisalkar, S. G.; Graetzel, M.; White, T. J. Synthesis and Crystal Chemistry of the Hybrid Perovskite (CH$_3$NH$_3$)PbI$_3$ for Solid-State Sensitised Solar Cell Applications. *J. Mater. Chem. A* **2013**, *1*, 5628–5641.

(13) Chi, L.; Swainson, I.; Cranswick, L.; Her, J.-H.; Stephens, P.; Knop, O. The Ordered Phase of Methylammonium Lead Chloride CH$_3$ND$_3$PbCl$_3$. *J. Solid State Chem.* **2005**, *178*, 1376–1385.

(14) Fabini, D. H.; Stoumpos, C. C.; Laurita, G.; Kaltzoglou, A.; Kontos, A. G.; Falaras, P.; Kanatzidis, M. G.; Seshadri, R. Reentrant Structural and Optical Properties and Large

Positive Thermal Expansion in Perovskite Formamidinium Lead Iodide. *Angew. Chem. Int. Ed.* **2016**, *55*, 15392–15396.

(15) Worhatch, R. J.; Kim, H.; Swainson, I. P.; Yonkeu, A. L.; Billinge, S. J. L. Study of Local Structure in Selected Organic–Inorganic Perovskites in the $Pm\bar{3}m$ Phase. *Chem. Mater.* **2008**, *20*, 1272–1277.

(16) Laurita, G.; Fabini, D. H.; Stoumpos, C. C.; Kanatzidis, M.; Seshadri, R. Chemical Tuning of Dynamic Cation Off-Centering in the Cubic Phases of Hybrid Tin and Lead Halide Perovskites. *Chem. Sci.* **2017**, *8*, 5628–5635.

(17) Fabini, D. H.; Laurita, G.; Bechtel, J. S.; Stoumpos, C. C.; Evans, H. A.; Kontos, A. G.; Raptis, Y. S.; Falaras, P.; der Ven, A. V.; Kanatzidis, M. G.; Seshadri, R. Dynamic Stereochemical Activity of the Sn^{2+} Lone Pair in Perovskite $CsSnBr_3$. *J. Am. Chem. Soc.* **2016**, *138*, 11820–11832.

(18) Beecher, A. N.; Semonin, O. E.; Skelton, J. M.; Frost, J. M.; Terban, M. W.; Zhai, H.; Alatas, A.; Owen, J. S.; Walsh, A.; Billinge, S. J. L. Direct Observation of Dynamic Symmetry Breaking above Room Temperature in Methylammonium Lead Iodide Perovskite. *ACS Energy Lett.* **2016**, *1*, 880–887.

(19) Wu, X.; Tan, L. Z.; Shen, X.; Hu, T.; Miyata, K.; Trinh, M. T.; Li, R.; Coffee, R.; Liu, S.; Egger, D. A.; Makasyuk, I.; Zheng, Q.; Fry, A.; Robinson, J. S.; Smith, M. D.; Guzelturk, B.; Karunadasa, H. I.; Wang, X.; Zhu, X.; Kronik, L.; Rappe, A. M.; Lindenberg, A. M. Light-Induced Picosecond Rotational Disordering of the Inorganic Sublattice in Hybrid Perovskites. *Sci. Adv.* **2017**, *3*, e1602388.

(20) Stoumpos, C. C.; Malliakas, C. D.; Kanatzidis, M. G. Semiconducting Tin and Lead Iodide Perovskites with Organic Cations: Phase Transitions, High Mobilities, and Near-Infrared Photoluminescent Properties. *Inorg. Chem.* **2013**, *52*, 9019–9038.

19

(21) Larson, A. C.; Dreele, R. V. General Structure Analysis System (GSAS). Los Alamos National Laboratory Report LAUR 86–748, 2004.

(22) Toby, B. H. *EXPGUI*, a Graphical User Interface for *GSAS*. *J. Appl. Crystallogr.* **2001**, *34*, 210–213.

(23) Momma, K.; Izumi, F. *VESTA3* for Three-Dimensional Visualization of Crystal, Volumetric and Morphology Data. *J. Appl. Crystallogr.* **2011**, *44*, 1272–1276.

(24) Mitzi, D.; Liang, K. Synthesis, Resistivity, and Thermal Properties of the Cubic Perovskite $NH_2CH=NH_2SnI_3$ and Related Systems. *J. Solid State Chem.* **1997**, *134*, 376–381.

(25) Dang, Y.; Zhou, Y.; Liu, X.; Ju, D.; Xia, S.; Xia, H.; Tao, X. Formation of Hybrid Perovskite Tin Iodide Single Crystals by Top-Seeded Solution Growth. *Angew. Chem. Int. Ed.* **2016**, *55*, 3447–3450.

(26) Hanusch, F. C.; Wiesenmayer, E.; Mankel, E.; Binek, A.; Angloher, P.; Fraunhofer, C.; Giesbrecht, N.; Feckl, J. M.; Jaegermann, W.; Johrendt, D.; Bein, T.; Docampo, P. Efficient Planar Heterojunction Perovskite Solar Cells Based on Formamidinium Lead Bromide. *J. Phys. Chem. Lett.* **2014**, *5*, 2791–2795.

(27) Zhumekenov, A. A.; Saidaminov, M. I.; Haque, M. A.; Alarousu, E.; Sarmah, S. P.; Murali, B.; Dursun, I.; Miao, X.-H.; Abdelhady, A. L.; Wu, T.; Mohammed, O. F.; Bakr, O. M. Formamidinium Lead Halide Perovskite Crystals with Unprecedented Long Carrier Dynamics and Diffusion Length. *ACS Energy Lett.* **2016**, *1*, 32–37.

(28) Koh, T. M.; Krishnamoorthy, T.; Yantara, N.; Shi, C.; Leong, W. L.; Boix, P. P.; Grimsdale, A. C.; Mhaisalkar, S. G.; Mathews, N. Formamidinium Tin-Based Perovskite with Low Eg for Photovoltaic Applications. *J. Mater. Chem. A* **2015**, *3*, 14996–15000.

(29) Lee, S. J.; Shin, S. S.; Kim, Y. C.; Kim, D.; Ahn, T. K.; Noh, J. H.; Seo, J.; Seok, S. I. Fabrication of Efficient Formamidinium Tin Iodide Perovskite Solar Cells through SnF_2−Pyrazine Complex. *J. Am. Chem. Soc.* **2016**, *138*, 3974–3977.

(30) Stroppa, A.; Sante, D. D.; Barone, P.; Bokdam, M.; Kresse, G.; Franchini, C.; Whangbo, M.-H.; Picozzi, S. Tunable Ferroelectric Polarization and its Interplay with Spin-Orbit Coupling in Tin Iodide Perovskites. *Nat. Commun.* **2014**, *5*, 5900.

(31) Waghmare, U. V.; Spaldin, N. A.; Kandpal, H. C.; Seshadri, R. First-Principles Indicators of Metallicity and Cation Off-Centricity in the IV-VI Rocksalt Chalcogenides of Divalent Ge, Sn, and Pb. *Phys. Rev. B* **2003**, *67*, 125111.

(32) Božin, E. S.; Malliakas, C. D.; Souvatzis, P.; Proffen, T.; Spaldin, N. A.; Kanatzidis, M. G.; Billinge, S. J. L. Entropically Stabilized Local Dipole Formation in Lead Chalcogenides. *Science* **2010**, *330*, 1660–1663.

(33) Jensen, K. M. O.; Božin, E. S.; Malliakas, C. D.; Stone, M. B.; Lumsden, M. D.; Kanatzidis, M. G.; Shapiro, S. M.; Billinge, S. J. L. Lattice Dynamics Reveals a Local Symmetry Breaking in the Emergent Dipole Phase of PbTe. *Phys. Rev. B* **2012**, *86*, 085313.

(34) Knox, K. R.; Božin, E. S.; Malliakas, C. D.; Kanatzidis, M. G.; Billinge, S. J. L. Local Off-Centering Symmetry Breaking in the High-Temperature Regime of SnTe. *Phys. Rev. B* **2014**, *89*, 014102.

(35) Yaffe, O.; Guo, Y.; Tan, L. Z.; Egger, D. A.; Hull, T.; Stoumpos, C. C.; Zheng, F.; Heinz, T. F.; Kronik, L.; Kanatzidis, M. G.; Owen, J. S.; Rappe, A. M.; Pimenta, M. A.; Brus, L. E. Local Polar Fluctuations in Lead Halide Perovskite Crystals. *Phys. Rev. Lett.* **2017**, *118*, 136001.

(36) Smith, M. D.; Jaffe, A.; Dohner, E. R.; Lindenberg, A. M.; Karunadasa, H. I. Structural

Origins of Broadband Emission from Layered Pb-Br Hybrid Perovskites. *Chem. Sci.* **2017**, *8*, 4497–4504.

(37) Fabini, D. H.; Hogan, T.; Evans, H. A.; Stoumpos, C. C.; Kanatzidis, M. G.; Seshadri, R. Dielectric and Thermodynamic Signatures of Low-Temperature Glassy Dynamics in the Hybrid Perovskites $CH_3NH_3PbI_3$ and $HC(NH_2)_2PbI_3$. *J. Phys. Chem. Lett.* **2016**, *7*, 376–381.

(38) Onoda-Yamamuro, N.; Matsuo, T.; Suga, H. Dielectric Study of $CH_3NH_3PbX_3$ (X = Cl, Br, I). *J. Phys. Chem. Solids* **1992**, *53*, 935–939.
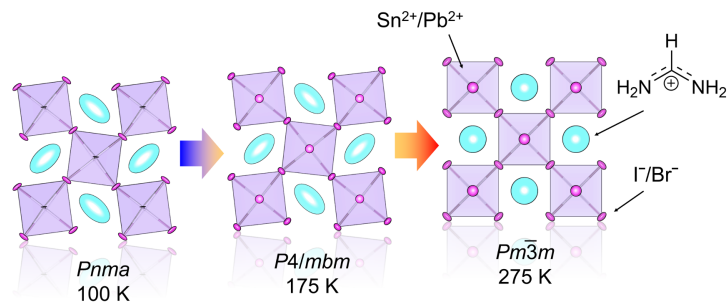
For Table of Contents use only

For Table of Contents only:

The temperature-dependent structure evolution of the hybrid halide perovskite compounds formamidinium tin iodide and formamidinium lead bromide has been monitored using synchrotron X-ray diffraction between $300\,\mathrm{K}$ and $100\,\mathrm{K}$. The data are consistent with a transition from cubic $Pm\overline{3}m$ to tetragonal $P4/mbm$ upon cooling; this occurs for FAPbBr$_3$ between $275\,\mathrm{K}$ and $250\,\mathrm{K}$, and for FASnI$_3$ between $250\,\mathrm{K}$ and $225\,\mathrm{K}$. Upon further cooling, between $150\,\mathrm{K}$ and $125\,\mathrm{K}$, both materials undergo a transition to an orthorhombic $Pnma$ structure.

23

Supporting Information

Crystal Structure Evolution and Notable Thermal Expansion in Hybrid Perovskites Formamidinium Tin Iodide and Formamidinium Lead Bromide

Emily C. Schueller,[†] Geneva Laurita,[‡] Douglas H. Fabini,[†]

Constantinos C. Stoumpos,[¶] Mercouri G. Kanatzidis,[¶] and Ram Seshadri[*,†,§]

[†]*Materials Department and Materials Research Laboratory*

University of California, Santa Barbara, California 93106, USA

[‡]*Department of Chemistry and Biochemistry, Bates College, Lewiston, Maine 04240, United States*

[¶]*Department of Chemistry, and Argonne-Northwestern Solar Energy Research Center*

Northwestern University, Evanston, Illinois 60208, USA

[§]*Department of Chemistry and Biochemistry*

University of California, Santa Barbara, California 93106, USA
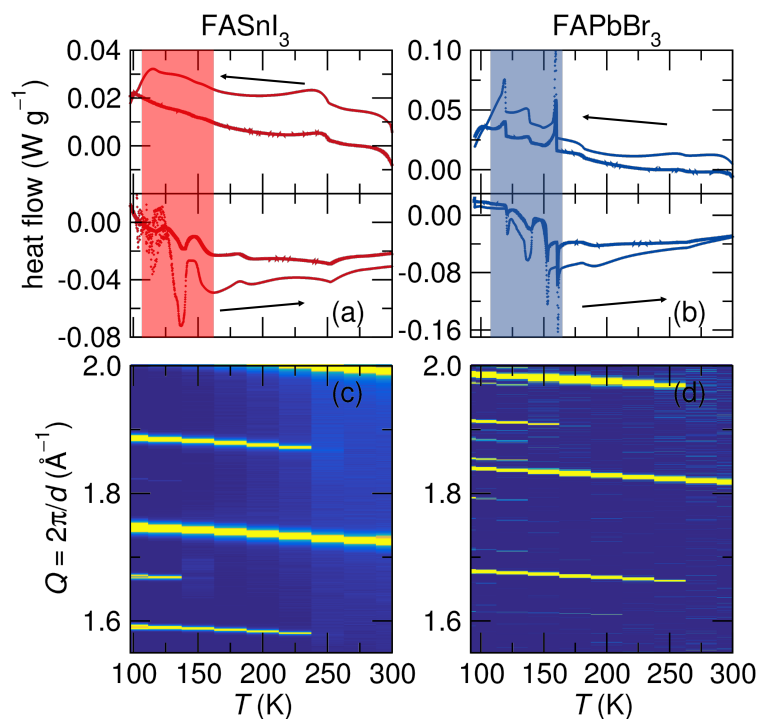
E-mail: seshadri@mrl.ucsb.edu

Figure S1: DSC from 100 K to 300 K confirms the presence of phase transitions for (a) FASnI$_3$ and (b) FAPbBr$_3$. The arrows indicate cooling and heating ramps. XRD data performed in the same temperature range for (c) FASnI$_3$ and (d) FAPbBr$_3$. Phase transitions upon cooling are signaled by the development of new peaks in the pattern, indicating a lowering of symmetry in the crystal structure. XRD patterns were taken at 25 K intervals, and the pattern is centered on the temperature at which it was taken. Phase transition temperatures are in agreement from DSC and XRD. Due to the complexity of the low temperature transition(s) in DSC, the regions of interest are shaded.